AN ADAPTABLE BIDIRECTIONAL BATTERY CHARGER FOR THE VARIATION OF ELECTRIC VEHICLES

B. Prasanna Kumar, UG Student, Sree Vahini Institute of Science and Technology (Autonomous), Tiruvuru, Andhra Pradesh
M. Anand, UG Student, Sree Vahini Institute of Science and Technology (Autonomous), Tiruvuru, Andhra Pradesh
T. Paparao, UG Student, Sree Vahini Institute of Science and Technology (Autonomous), Tiruvuru, Andhra Pradesh
D. Bikshalu UG Student, Sree Vahini Institute of Science and Technology (Autonomous), Tiruvuru, Andhra Pradesh
Mr. G. Chitti Babu Assist. Professor, Dept of EEE, Sree Vahini Institute of Science and Technology (Autonomous), Tiruvuru, Andhra Pradesh
Dr. K. Kiran Kumar Assoc. Professor, Dept of EEE, Sree Vahini Institute of Science and Technology (Autonomous), Tiruvuru, Andhra Pradesh

Abstract:
This study presents the design and functioning of a modified SEPIC converter-based bidirectional battery charger for a variety of EVs. Electric two-wheelers (e2W) and electric cars are among several types of EVs. In order to charge an e2W with a 72 V battery and an electric automobile with a 240 V battery, a modified SEPIC converter is designed. The main benefit of the battery charger which is being provided is that it complies with the IEC standard and provides good charging function. Additionally, bidirectional functioning is a benefit of the improved SEPIC converter-based battery charger. Grid to Vehicle (G2V) analysis is performed using the optimal grid voltage to attempt to confirm the efficacy of the proposed battery charger grid. Furthermore, the charger effectiveness is confirmed using amplitude changes in the grid voltage. Finally, a vehicle-to-home (V2H) operation is conducted to examine the effectiveness of the provided charger during the bidirectional operation.

Key words:
Power quality, DC/DC converter, AC/DC converter, and battery charger.

I. Introduction

Battery charger technology is now advanced to the stage where it can be divided into two categories: unidirectional and bidirectional. The goal of the most recent unidirectional battery chargers [1]– [3] is to boost power density. In this regard, the bridgeless battery charger architecture for low voltage battery-powered electric vehicles (EVs) is described by the authors in [1]. This charger's excellent efficiency and high-power density are its advantages. The authors in [2] have introduced a single-stage EV charger for high voltage battery-powered EVs that is based on resonant converters, keeping high efficiency in view. The proposed EV charger features the benefit of reduced losses, which translates into great efficiency. In [3], a different architecture for a battery with a very high voltage is provided. Nevertheless, the EV charger topologies shown above are unidirectional.

Modern bidirectional battery chargers [4]– [5] significantly improve EV practicality while operating vehicle-to-grid/home (V2G or V2H). A bidirectional EV charger architecture was proposed by the authors on [4] in regard to it. The provided charger conforms with the relevant power quality requirements and enables four-quadrant operation [5]. An electrolytic capacitor-less EV charger architecture with sinusoidal ripple charging was introduced by the authors in [6]. The authors have also discussed about the benefits of sinusoidal ripple current charging. Nevertheless, the bidirectional topologies described above are two-stage topologies. As a result, compared to single stage topologies, the losses are much higher. In addition to their efficiency, the charger topologies covered above are only appropriate for a limited output voltage range. Consequently, research should be done on EV chargers with an extensive output voltage range. Modern EV chargers with wide output voltage ranges are examined in [7]– [8] with this in perspective. A Vienna converter-based EV charger is shown in

[7]. According to the authors, the given topology's primary benefit is its extensive output voltage range capabilities. It is a unidirectional EV charger, though. In [8], the authors introduced a topology that can operate in both directions and provides a wide output voltage range. Nonetheless, the EV charger architecture which is being presented is a two-stage EV charger.
A single-stage bidirectional battery charger with an extensive output voltage range is presented in this study in consideration of the deficiencies of the aforementioned current EV charge topologies. Furthermore, the battery charger which is being offered isolates the vehicle battery from the AC source galvanically. The following represents the text essential advancement.

- A modified SEPIC converter-based bidirectional battery charger with a wide output voltage range is demonstrated, along with its design and functionality.
- The control and operational concept of the charger topology which is being given are examined.
- For demonstrate the effectiveness of the suggested charger during grid-to-vehicle (G2V) operation, a 1.1 kW system is implemented.
- A 72 V and 240 V battery at the output are used to confirm the performance of the charger which is being supplied. Electric two-wheeler (e2W) charging in a house is analogous to the charging process of a 72 V battery. Additionally, the 240 V battery charging process is equivalent to charging an electric vehicle at home.
- The efficacy of the proposed charger is confirmed by presenting its performance with fluctuations in grid voltage.
- The effectiveness of the proposed charger during the bidirectional operation is confirmed by discussing the V2H operation with a 240 V battery system.

II. Configuration of the system
Fig. 1 shows the proposed EV charger system. The charger which is being displayed is clearly the result of integrating two modified SEPIC bidirectional converter cells. The SEPIC converter cells function in two ways: one during the grid voltage positive half cycle and another during its negative half cycle. Thus, the current improved SEPIC converter-based AC/DC converter functions as a bridgeless bidirectional converter. The converter used uses an RC filter to eliminate switching noise from the grid voltage. Furthermore, when power is transferred from the AC supply to the EV battery, the input inductor Lin is activated to maintain grid current regulation. Interestingly, this charger utilizes the use of a high-frequency transformer. Galvanic isolation between the battery and the AC source is provided by the transformer. This transformer is designed in a way that allows its magnetizing inductance to function in the discontinuous conduction mode (DCM). Therefore, a unity power factor at supply is implemented by this transformer DCM function. Thus, the charger which is being offered satisfies the relevant power quality standard and has features such an expansive output voltage range and the capacity to flow power in both directions.

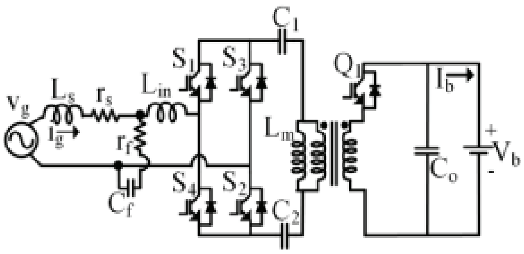

Fig. 1 shows the charger circuit diagram.

III. Concept of performance
The battery current remains constant during the G2V charging process by the charger which is being offered. Additionally, it controls the sinusoidal voltage during V2H operation at the common intersection of the charger and load. Figs. 2-3 show the circuit diagrams which describe the component states and related waveforms, putting these operations in perspective. It is important to observe that the current charger positive half-cycle and negative half-cycle operating modes are comparable for

 ISSN: 2278-4632
Vol-15, Issue-04, No.02, April: 2025

both G2V and V2H operations, as shown in Figs. 2(a)–(f). According to this perspective, the G2V processes during the positive half-cycle are described as entirely follows.

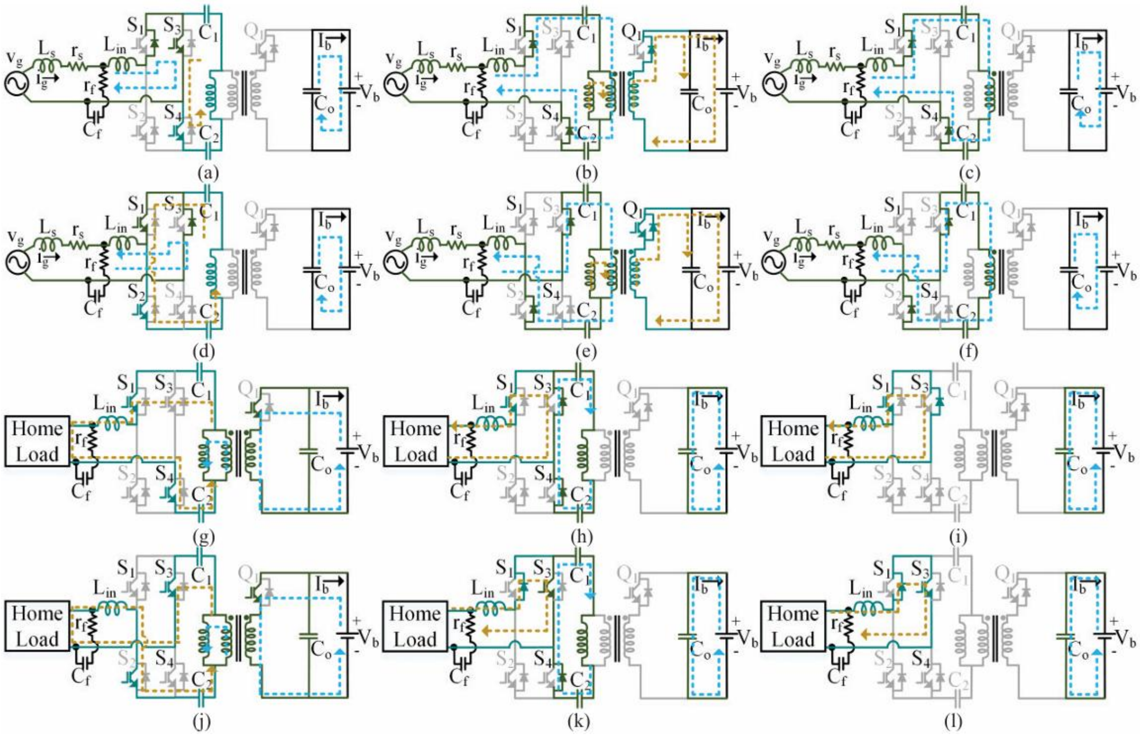

Fig.2 shows the EV charger operating modes when charging (a)–(c) during the grid voltage positive half cycle and (d)–(f) during its negative half cycle.

Mode I: This mode is initiated by turning switches S3 and S4 "ON" during the grid voltage positive half cycle. Since the anti-parallel diode of switch S1 is forward biased, as shown in Fig. 2(a), the inductor Lin begins to charge via this diode and switches S3. Additionally, switches S3 and S4 allow the capacitors C1 and C2 to discharge. The transformer magnetizing inductor receives the stored energy from capacitors C1 and C2. Thus, as seen in Fig. 2(a), the magnetizing inductance, Lm, begins to charge. As seen in Fig. 2(a), the battery receives the energy stored in the output capacitor. Particularly, Fig. 3(a) displays the switching pulses as well as the corresponding inductor current and capacitor voltage waveforms.

Mode II: When switches S3 and S4 are switched off, mode-I gives the ability to mode-II. In this mode, the transformer action transfers the energy stored in the high-frequency transformer's magnetizing inductance to the battery. Capacitors C1 and C2 receive the stored inductor energy in Lin when switches S3 and S4 are off, as shown in Fig. 2(b). Consequently, this mode initiates the charging of these capacitors. This mode stops when the magnetizing inductance is fully discharged since the transformer functions in DCM. Fig. 3(a) shows the waveforms associated with this process.

Mode III: The transformer stops functioning because the magnetizing inductance is entirely drained. Consequently, no power is transmitted from the AC supply to the battery during this functioning mode; instead, capacitors C1 and C2 charge via the AC supply. In this mode, the output capacitor stored energy is used to charge the battery. Figures 2 and 3 show the circuit diagram and important waveforms. The V2H operation is used to illustrate the supplied charger bidirectional function. Taking note of this, Figs. 2(g)–(l) display the circuit diagrams of the operating modes during the V2H operation. As the operating modes throughout the two-grid voltage half-cycles are significantly the same, the following provides a detailed description of the V2H operation during the positive half-cycle.

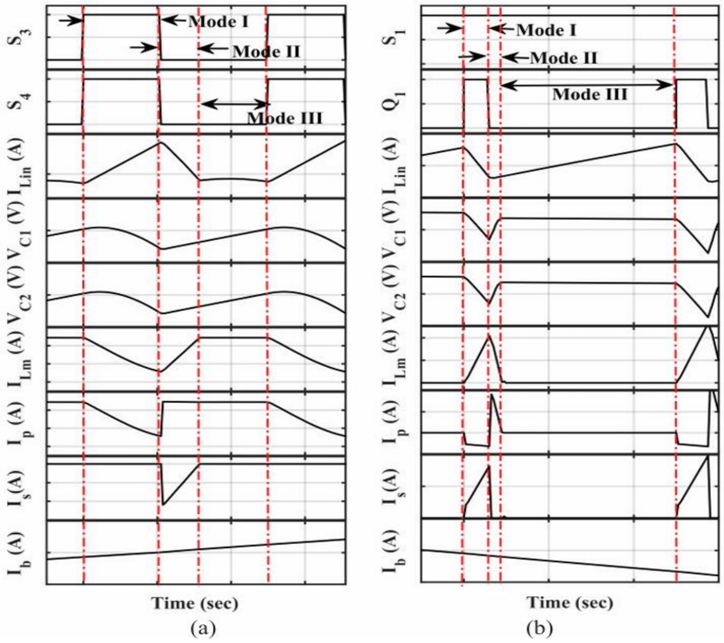

Fig. 3 Operating state waveforms.

Mode I: This mode begins when switch Q1 is turned "ON," taking into account the V2H functioning at steady-state. The transformer magnetizing inductance becomes activated. Additionally, the energy stored in the vehicle battery and capacitors C1 and C2 is used to supply power to the household loads. In this state, the switches S1 and S4 are "ON." Fig. 2(g) shows the accompanying circuit diagrams which describe such action, and Figure 3(b) shows the related waveforms.

Mode II: This mode begins when switch Q1 is switched off, such as in the prior mode. Capacitors charge using the stored energy in magnetizing inductance when the diodes of switches S3 and S4 conduct in this mode, as shown in Fig. 2(h). Furthermore, as shown in Fig. 2(h), the power to household loads is provided by the stored energy in the inductor Lin. In Fig. 3(b), the corresponding waveforms are displayed.

Mode III: The capacitor is charged when the magnetizing inductance decreases. In this functioning state, as shown in Fig 2(i), the inductor Lin stored energy is used to supply the house loads. The operation waveforms are displayed in Fig. 3(b).

IV. Design of the system

The charger component is selected based on the rated parameters and the modes of operation listed above. Table I provides these rating parameters. Furthermore, Table I provides the calculated and specified values of the components for permitted voltage and current ripples. Interestingly, the maximum battery voltage at the output and the rated supply at the input are used to accomplish the charging operation at the rated condition. Consequently, the rated input voltage and maximum output voltage are taken into account while calculating the converter duty ratio. This duty ratio is used to compute the other parts of the charger which is being provided.

Table I: Estimation of Parameters

Parameters	Design estimation	Remarks	Estimated value	Selected Value
L_{in}	$\frac{V_{g,max}D_{max}}{f_s\Delta i_{in}}$	D=0.28; f_s =20KHz;Δi_{Lin}=30% of i_{Lin}	2.32mH	3mH
$L_{m,c}$	$\frac{R_{L\,min}}{f_s(1+\frac{2D}{D_c})}$	f_s =20KHz;$R_L=\frac{V_b}{I_b}$	0.3mH	60µH
$C_1 = C_2$	$\frac{1}{((2\pi f_{res})^2 \times (L_{in}+L_m))}$	f_{res} =2KHz;L_m=60µH	2.59µF	3µF

 ISSN: 2278-4632
Vol-15, Issue-04, No.02, April: 2025

C_0	$\frac{P}{2 \times \omega \times V_{DC} \times v_{rip}}$	V_{rip}=10% of V_{DC}=72V	4605.2µF	4700µF

V. CONTROL ALGORITHM

The controller block diagrams for G2V and V2H operations are shown in Figs. 4(a)–(b). Balancing battery current during this operation and controlling power quality in accordance with relevant standards are the objectives of the controller design. According to this perspective, the converter transformer is built to function in DCM. Furthermore, the transformer DCM operation verifies which the grid current quality satisfies with the relevant power quality standard. thereby, during G2V operation, the controller main objective is to sustain the current flowing at the battery terminals. Additionally, during V2H operation, the controller of the charger which is being provided is in responsibility of maintaining the voltage at the common intersection of the load and the charger.

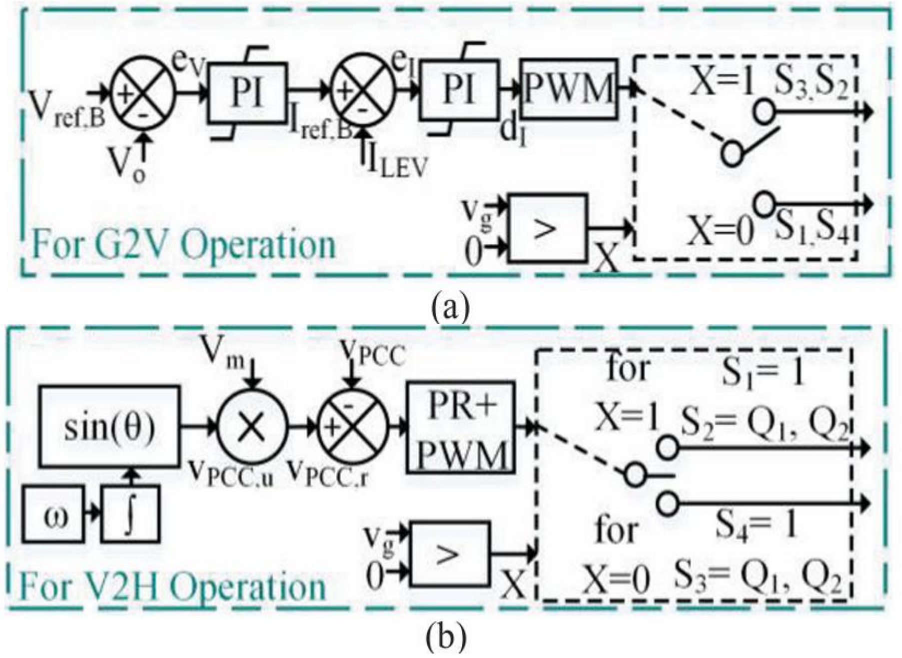

Fig. 4 Diagram of the control block.

Controller for G2V operations

A constant current charging current algorithm controls the G2V functioning. Fig. 4(a) shows the control block diagram. Here, as shown in Fig. 4(a), the battery current is measured and contrasted with the reference charging current. The proportional-integral (PI) regulator optimizes the difference between the measured and reference battery current. As shown in Fig. 4(a), this PI regulator uses a pulse width modulation switching (PWM) technique to analyze the error and compute the reference duty ratio. The switch pairs S1-S2 get these switching pulses during the grid voltage negative half cycle, while S3-S4 receive them during its positive half cycle. Particularly, the comparator and measured grid voltage are used to estimate the positive and negative half cycle durations.

Controller for the V2H System

The control technique is in charge of regulating the sinusoidal voltage at the point of common intersection (PCI) of the load and the charger during the V2H operation, as illustrated in Fig. 4(b). This is accomplished by creating a reference voltage and comparing it to the voltage that was measured at the PCI. Interestingly, the proportional resonance (PR) regulator receives the computed error. The estimated output is used for pulse width modulation (PWM) switching after it has been processed by the PR regulator. Switches S1 and S2 are controlled by this controller in accordance with the positive half cycle and a negative half cycle of the grid voltage, respectively, whereas switches Q1-S4 are controlled in pairs. Additionally, the comparator and measured reference sinusoidal voltage are used to estimate the positive and negative half cycle periods.

VI. Results and Discussion

ISSN: 2278-4632
Vol-15, Issue-04, No.02, April: 2025

An analysis of the provided charger performance is conducted under both ideal and variable grid voltage settings. Within this context, the charger expansive output voltage range functioning is verified by the G2V operation with a 72 V and 240 V battery. The results of this study are shown in Figs. 5-7. Moreover, Figs. 8(a)–(b) display the results of testing the effectiveness of the G2V operation with different amplitudes of the AC supply voltage. Additionally, the outcomes are shown in Figs. 9(a)-(b), which support the provided charger satisfying behavior during the V2H operation. This is an extensive discussion of the aforementioned observations.

Battery charging applying 72 V and 240 V

Two batteries, one at 72 V and the other at 240 V, are charged for the purpose to assess the effectiveness of the stated charger with its extensive output voltage range performance. The outcomes are displayed in Fig. 5. The grid voltage and current are in phase when charging a 72 V battery in a low voltage battery-powered vehicle, as can be seen clearly in Fig. 5(a). Interestingly, the reference current is used to regulate the average battery current. Additionally, the battery current ripples adhere to the relevant norms [9]. Also, because grid current THD is 3.46%, Fig. 5(a) shows compliance with the relevant grid current quality criteria.

Fig. 5(b) illustrates the 240 V battery's charging process. In-phase grid voltage and current are displayed below. Additionally, Fig. 5(b) provided the battery voltage. Fig. 5(b) illustrates the procedure to regulate the average battery current when charging a 240 V battery. The controller design is satisfactory since the ripples in the battery current fall within the parameters specified pertain. Additionally, the grid current THD is 1.11%, signifying that the operation complies with the relevant performance criteria. The charger design and control algorithm are therefore adequate.

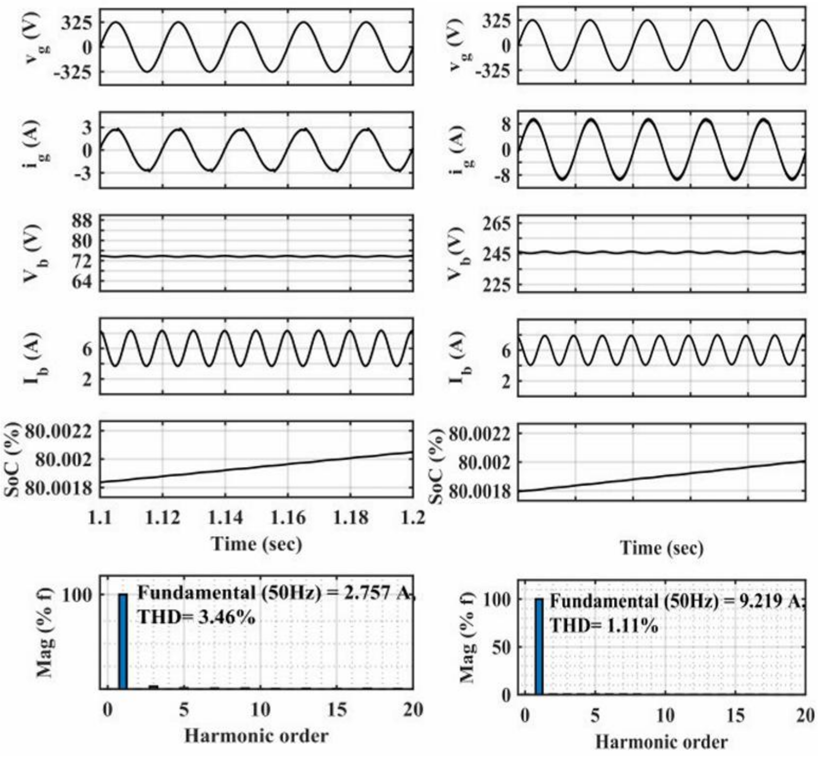

(a) (b)

Fig. 5. Outcomes of controlled charging operations using (a) 72 V battery and (b) 240 V battery.

Analysis of Charger Functionality During G2V Operation

In Fig. 6(a), the voltage and current strains on the charger components during G2V operation with a 72 V battery-powered vehicle are clearly seen. As seen in Fig. 6(a), the input inductor current iLin is followed by the grid current. The voltages, VC1 and VC2, are well-regulated, and the capacitors C1 and C2 function in continuous conduction mode, as shown in Fig. 6(a). Moreover, Fig. 6(a) shows that the high frequency transformer magnetizing inductance functions in discontinuous conduction mode (DCM). Therefore, the converter design for charging batteries at 72 V is sufficiently.

The voltage and current strains on the charger passive components during a 240 V battery charge are shown in Fig. 6(b). When charging a high-voltage battery, power transmission rises, increasing the

 ISSN: 2278-4632
Vol-15, Issue-04, No.02, April: 2025

current stress via the input inductor, Lin. During this procedure, the voltage between capacitors C1 and C2 is notably controlled. The waves in the capacitor voltage are greater than when a 72 V battery is being charged. Additionally, Fig. 6(b) illustrates the verification of the transformer magnetizing inductance DCM function. Because the components currents and voltages are controlled, the charger design is adequate.

The voltage and current across the switches are examined in addition to the passive components, and the findings are displayed in Figs. 7(a)–(b). Notably, during the wide voltage range operation, the voltages and currents across and through the switches during G2V operation remain within the design parameters. Therefore, the charger design and control algorithm are proper.

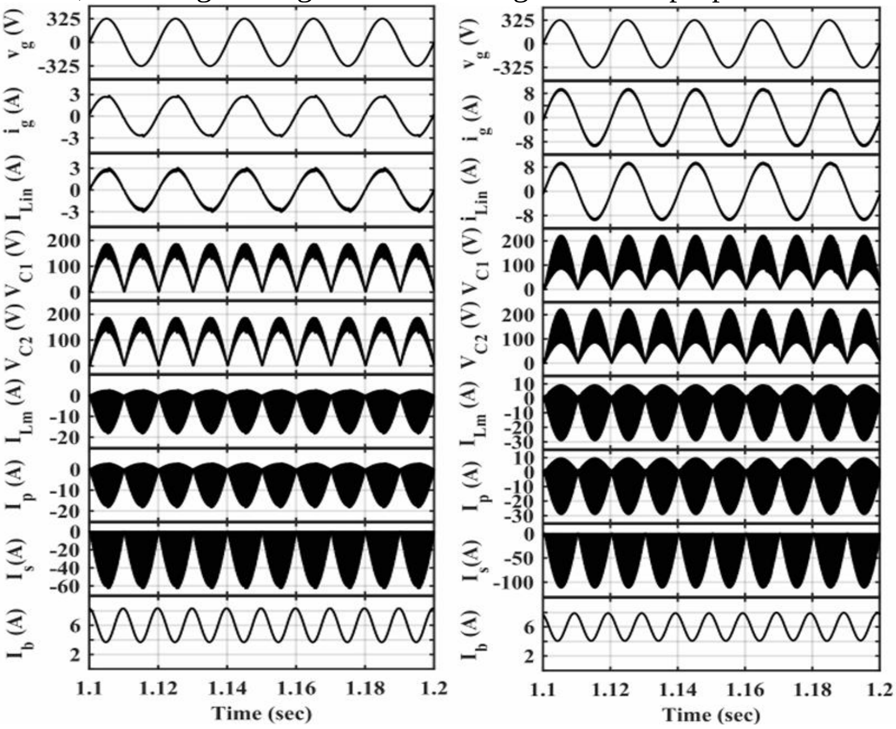

(a) (b)

Fig. 6 Voltage and current stresses during the charging operation with (a) 72 V battery and (b) 240 V battery.

Charger Performance with Varying Grid Voltage

The charger effectiveness under poor conditions is evaluated by considering into consideration fluctuations in the grid voltage amplitude. During the voltage sag procedure, a significant 20% drop in the grid voltage is taken into consideration. The grid current increase is a reflection of the grid voltage decrease, as seen in Fig. 8(a). As a result, the charging process is kept running at constant current. Moreover, as shown in fig. 8(a), the grid current THD is 1.59%, indicating that it complies with the relevant power quality requirement. Fig. 8(b) shows the outcomes of the charging operation between the grid voltage well and the charger which is being provided. As seen in Fig. 8(b), the grid current drops as the grid voltage spikes. As seen in Fig. 8(b), this results in the uninterrupted charging operation. Additionally, throughout the procedure, a 2.65% grid current THD is obtained. As a result, the grid current complies with the relevant power quality criteria

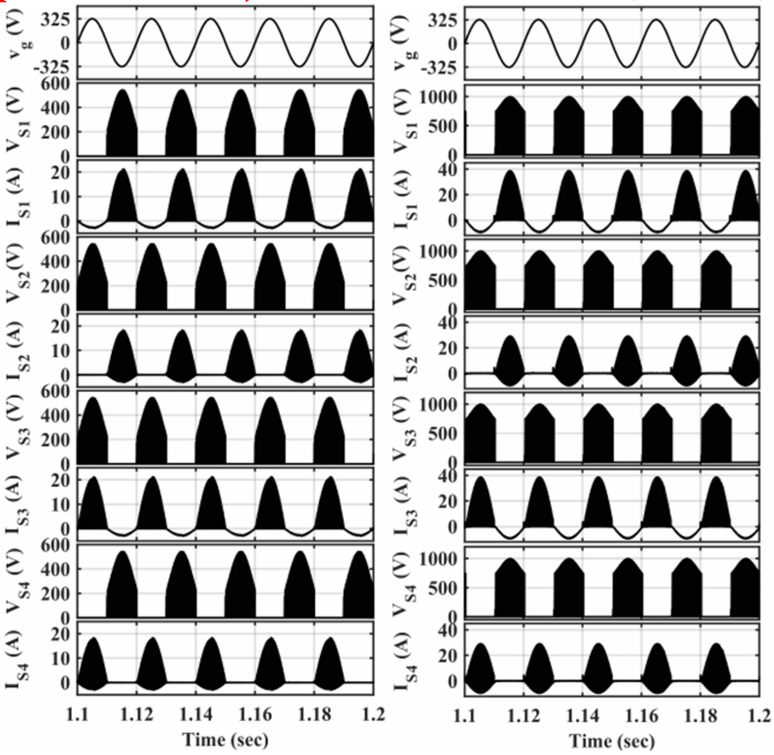

(a) (b)

Fig. 7 Voltage and current stresses during the charging operation with (a) 72 V battery and (b) 240 V battery.

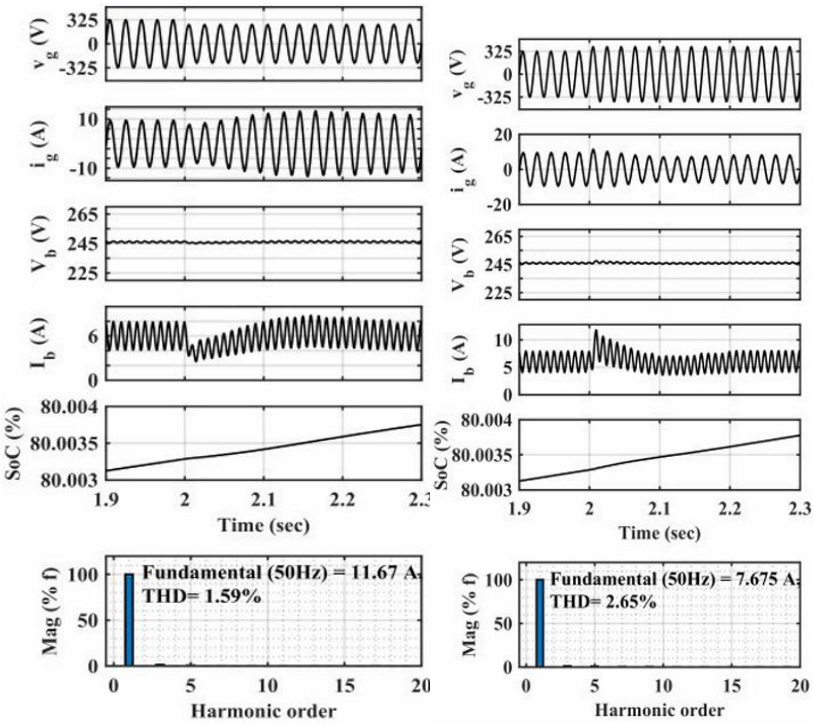

(a) (b)

Fig. 8. Grid voltage operation during (a) sag and (b) swell.

Performance Evaluation for V2H Activities

The V2H operation is carried out for the purpose to evaluate the efficacy of the proposed charger during the bidirectional operation and the outcomes are shown in Figs. 9(a)-(b). The sinusoidal voltage remains unchanged at the common intersection of the load and the charger, as shown in Fig. 9(a). Fig. 9(a) shows the non-linear load current. The voltage and current of the out-of-phase load confirm that the load is receiving electricity. As seen in Fig. (9a), the battery current is negative and controlled. Consequently, the load receives its power from the battery. During the V2H operation, the voltage and current across the passive parts of the charger are shown in Fig. 9(b). Fig. 9(b) presents it as clear that these currents and voltages are controlled. As a result, during the V2H operation, the provided charger performs properly.

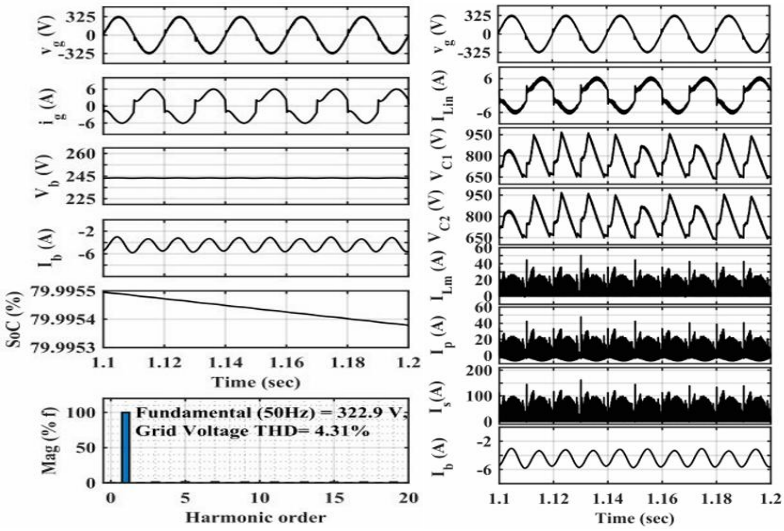

(a) (b)

Fig. 9 Outcomes during the V2H operation

CONCLUSION

A bidirectional battery charger that is separated and features a vast output voltage range is demonstrated. A modified SEPIC converter-based bidirectional bridgeless converter is used to construct the charger which is being exhibited. The converter fundamental DC functioning is covered. The ability to regulate the battery current during both V2H and G2V operation is also exhibited. Simulation is used to verify and validate the provided charger design and effectiveness during G2V and V2H operations. The charging of a 72 V and 240 V battery is being done in order to confirm the extensive output voltage functionality. Furthermore, the controller efficacy has been confirmed across a range of grid voltage scenarios. During the grid-connected operation, the charger is adhered to the relevant power quality criteria. Finally, a successful V2H operation has been shown. Therefore, the offered charger design and functionality are deemed suitable.

REFERENCES

[1] R. Kushwaha, B. Singh and V. Khadkikar, “An Isolated Bridgeless Cuk– SEPIC Converter-Fed Electric Vehicle Charger,” IEEE Trans. on Ind. App., vol. 58, no. 2, pp. 2512-2526, March-April 2022.
[2] H. Nazi, E. Babaei, S. Tohidi and M. Liserre, “An Isolated SRC-Based Single Phase Single Stage Battery Charger for Electric Vehicles,” IEEE Trans. Transp. Elect., Early Access, 2022.
[3] M. Abbasi, K. Kanathipan and J. Lam, “An Interleaved Bridgeless Single-Stage AC/DC Converter with Stacked Switches Configurations and Soft-Switching Operation for High Voltage EV Battery Systems,” IEEE Trans. on Ind. App., Early Access, 2022.
[4] M. Restrepo, J. Morris, M. Kazerani and C. A. Cañizares, “Modeling and Testing of a Bidirectional Smart Charger for Distribution System EV Integration,” IEEE Trans. on Smart Grid, vol. 9, no. 1, pp. 152-162, Jan. 2018.
[5] A. Fernandez, J. Sebastian, M. M. Hernando, P. Villegas and J. Garcia, “Helpful hints to select a power-factor-correction solution for low- and medium-power single-phase power supplies,” IEEE Trans. on Ind. Elect., vol. 52, no. 1, pp. 46-55, Feb. 2005.
[6] M. Kwon and S. Choi, “An Electrolytic Capacitorless Bidirectional EV Charger for V2G and V2H Applications,” IEEE Trans. on Power Elect., vol. 32, no. 9, pp. 6792-6799, Sept. 2017.
[7] A. Jain, K. K. Gupta, S. K. Jain and P. Bhatnagar, “A Bidirectional Five Level Buck PFC Rectifier with Wide Output Range for EV Charging Application,” IEEE Trans. on Power Elect., 2022.
[8] Y. Yuan and Z. Zhang, “A Single-phase Vienna Rectifier with Wide Output Voltage Range,” IEEE Trans. Transp. Elect., Early Access.
[9] R. Kushwaha and B. Singh, “A Bridgeless Isolated Half Bridge Converter Based EV Charger with Power Factor Pre-regulation,” IEEE Transp. Elect. Conf. (ITEC-India), pp. 1-6, 2019.

